Porphyrin based metal–organic framework films: nucleation and growth†

Zhenyu Zhou,[ab] Soumya Mukherjee,[ab] Julien Warnan,[ab] Weijin Li,*[ab] Suttipong Wannapaiboon,[c] Shujin Hou,[de] Katia Rodewald,[bf] Bernhard Rieger,[bf] Peter G. Weidler,[g] Christof Wöll[g] and Roland A. Fischer*[ab]

Integration of porphyrin based metal organic frameworks (PP-MOFs) on a solid surface has emerged as a key advancement in terms of exploring their promising applications. However, a great challenge remains unmet when it comes to successfully fabricating a PP-MOF film with crystallinity, controllable orientation, adjustable morphology and thickness, all sustained in one. Herein, for the first time, vapor-assisted conversion (VAC) was developed as a facile and versatile technique to fabricate functional PP-MOF films on various substrates related to different application requirements. To understand the nucleation and growth mechanism, a number of fabrication methods were leveraged to prepare the PP-MOF films, thanks to an assortment of PP-MOFs varying from two-dimensional (2D) to three-dimensional (3D) scaffolds. The studies show that PP-MOF films are likely to display different nucleation and growth processes following different deposition approaches. This study demonstrates the pros and cons of different methods in the fabrication of functional PP-MOF films, potentially offering critical tools and reference points for the preparation of next-generation functional MOF thin films in general.

1. Introduction

Metal–organic frameworks (MOFs) are composed of organic linkers and inorganic metal nodes (or clusters) to afford potentially porous metal–organic nanospace.[1] Thanks to their modular composition amenable to reticular chemistry, good thermal stability and high surface areas, well-defined MOFs with tailored functionalities have drawn enormous attention in the fields of chemistry and materials science.[2] As a sub-class of MOFs, porphyrin-based MOFs (PP-MOFs) are known for their specific potential in catalysis and photoelectric devices, largely favoured because of their conjugated macrocyclic structures.[3–5] Considering practicality to serve diverse applications, integration of MOFs in the form of films onto a solid surface is a desired advancement. In fact, the fabrication of PP-MOFs as thin films could exploit the inherited merits of PP-MOFs as films, in order to show their promising applications in photovoltaics,[3] sensors,[6] and (photo)electrocatalysis.[7,8] To date, a number of MOF film preparation methods, such as seeding growth,[9] dip-coating,[10] electrochemical deposition,[11] layer-by-layer (LBL) deposition,[12,13] and solvothermal approaches,[8,14–16] have been developed for depositing MOFs onto various substrates. However, a systematic study of the pros and cons of these methods in the fabrication of PP-MOF films remains to be addressed.

Of late, a number of reports have surfaced that cover the emerging topic of preparing application-ready PP-MOF films. For instance, methods such as Langmuir–Blodgett layer-by-layer (LB-LBL) assembly,[17,18] modular assembly,[19] and spray liquid-phase epitaxy (SP-LPE)[20,21] have been developed to prepare crystalline 2D PP-MOF films. However, these either require a special deposition set-up, or need pre-treatments such as the formation of a well-ordered seed layer on the surface or heavily rely upon the functional groups of the substrate surface, impeding their potential scale-up and consequent applications. Regarding the fabrication of 3D PP-MOF films, it turns out to be a more complicated challenge. Although LBL[22] and inkjet printing methods[7] have been reported to prepare 3D PP-MOF films, the crystallinity and orientation of the films are far from satisfactory. Thus far, the solvothermal method is the most common approach and using it enables the growth of PP-

[a]Chair of Inorganic and Metal Organic Chemistry, Catalysis Research Center, Ernst Otto Fischer Straße 1, 85748 Garching b. Munchen, Germany
[b]Department of Chemistry, Technical University of Munich, Lichtenbergstraße 4, 85748 Garching b. Munchen, Germany. E mail: roland.fischer@tum.de; wj.li@tum.de
[c]Synchrotron Light Research Institute (Public Organization), Nakhon Ratchasima 30000, Thailand
[d]Physics of Energy Conversion and Storage, Department of Physics, James Franck Straße 1, 85748, Garching b. Munchen, Germany
[e]Catalysis Research Center, Otto Fischer Straße 1, 85748, Garching b. Munchen, Germany
[f]Wacker Chair of Macromolecular Chemistry, Catalysis Research Center, Ernst Otto Fischer Straße 1, 85747 Garching b. Munchen, Germany
[g]Institut fur Funktionelle Grenzflachen (IFG), Karlsruher Institut fur Technologie (KIT), 76021 Karlsruhe, Germany

† Electronic supplementary information (ESI) available. See DOI: 10.1039/d0ta06052f

MOF films.[8,14 16] However, it suffers from downsides: time and energy consumption combined with a weak control of the surface morphology (*e.g.*, roughness, grain size and distribution) and thickness. A great challenge exists with regard to the fabrication of a PP-MOF film that synergistically combines good crystallinity, controllable orientation, adjustable morphology and thickness.

Herein, a vapour-assisted conversion (VAC) method was developed to fabricate 2D and 3D PP-MOF films deposited on various substrates, such as gold/silicon/ITO substrates. The VAC method is based on the conversion of precursors by casting a solution layer on substrates to form a continuous crystalline film, largely credited to an exposure of precursors to the vapours from specific modulators at moderate temperatures.[23] We demonstrate that, while delivering a high quality thin film, this approach remains straightforward and versatile.

To further understand the nucleation and growth mechanism in PP-MOF films, three other typical methods such as solvothermal, modular assembly and LPE (Scheme 1) have been investigated in parallel with the VAC approach. All of these methods share a common aim: leaning forward towards the fabrication of 2D and 3D PP-MOF films. Grazing incidence X-ray diffraction (GIXRD), scanning electron microscopy (SEM), and environment-controlled quartz crystal microbalance (BEL-QCM) were used to study the characteristics such as crystallinity, orientation, morphology, thickness and porosity to evaluate the pros and cons of each method towards nucleation and growth in functional PP-MOF films. This resulted in a unique back-to-back investigation of the mechanisms involved in the nucleation and growth of PP-MOF films. Well-known 2D PP-MOFs such as Zn_2(ZnTCPP) (TCPP, tetrakis(4-carboxyphenyl)-porphyrin) and 3D PP-MOFs such as PCN-222 (PCN, porous coordination network), PCN-224 and MOF-525 have been used as typical examples to investigate the nucleation and growth of porphyrin-based MOF films.

2. Results and discussion

2.1. Preparation and characterisation of 2D PP-MOF films

Until recently, many 2D PP-MOFs have been fabricated as films to explore promising applications.[3,6,24 27] As a commonly studied 2D PP-MOF with a well-known simple composition, Zn_2(ZnTCPP) was selected as a prototype to investigate the nucleation and growth mechanisms in 2D PP-MOF films. Zn_2(ZnTCPP) comprises Zn(II)-centered TCPP (ZnTCPP) units linking binuclear Zn paddlewheel metal nodes $Zn_2(COO)_4$, affording a 2D "checkerboard" structure (Fig. S1a–c†). Along the *ab* plane, Zn(II) residing inside porphyrin units gets coordinated to the zinc atoms in the paddlewheel units. These classical "checkerboard" layers are further stacked in an AA packing arrangement, leading to the 2D PP-MOF structure (Fig. S1d and Table S1†). According to the literature studies detailing the preparation of paddlewheel structure based MOF films,[17,28,29] the MOF Zn_2(ZnTCPP) could indeed serve as a good candidate

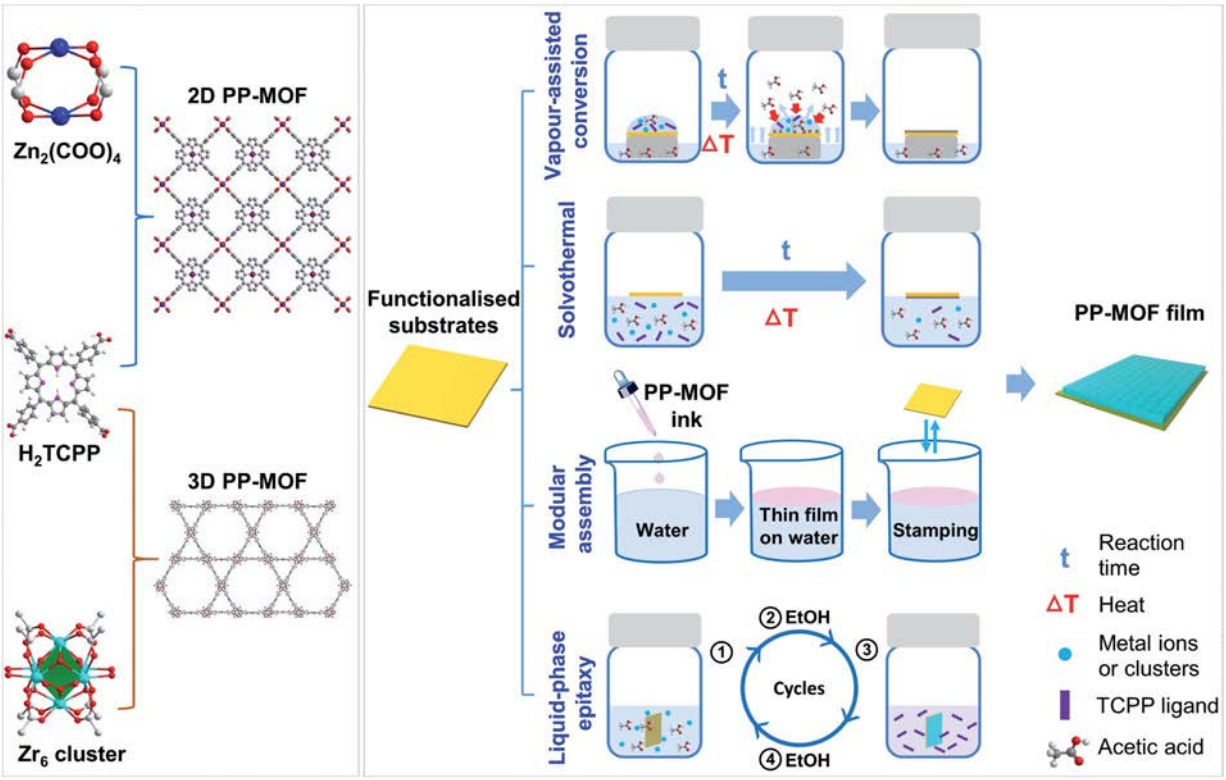

Scheme 1 Schematic representation of 2D and 3D PP-MOF films deposited on carboxylate-terminated gold substrates *via* diverse methods: vapour-assisted conversion; solvothermal; modular assembly; liquid-phase epitaxy. The left side comprises the building units and crystal structures of the 2D Zn_2(ZnTCPP) and 3D PCN-222, on the top and at the bottom, respectively.

to conduct our intended study: that is to study nucleation and growth processes in prototypal 2D PP-MOF films.

To begin with, VAC was employed to prepare Zn_2(ZnTCPP) MOF films. Subsequently, solvothermal, modular assembly and LPE methods all were used separately to prepare Zn_2(ZnTCPP) MOF films to draw rational comparisons with VAC. Different substrates are supposed to show different surface behaviours to initiate different nucleation and growth mechanisms in the resulting MOF films. Meanwhile, considering their practical uses, PP-MOFs need to be deposited on specific substrates. For example, microelectronic devices usually require the PP-MOF to be deposited on a gold surface;[5] whereas electrocatalytic devices or semiconductor devices need deposition on conductive ITO glass and silicon substrates, respectively.[7,30] Therefore, a variety of potential substrates with distinct surface functional groups will be examined with respect to their relative suitability towards the nucleation and growth of the corresponding PP-MOF films. Unless otherwise mentioned, PP-MOF films in the following discussion refer to films that were deposited on a carboxylate-terminated gold surface.

In each of our VAC experiments, a mixture of *N*,*N*-dimethylformamide (DMF) and acetic acid (v/v: 200 : 1) was used as the vapour source and a substrate (1 × 1 cm) was placed on a platform in a glass vial (Scheme 1). The reactants $Zn(NO_3)_2 \cdot 6H_2O$, TCPP and modulator acetic acid were dissolved in a binary mixture of DMF and ethanol (v/v: 3/1) as the precursor solution (Table S2†). Then, a droplet of this precursor solution was evenly deposited on the substrate. The vial, upon sealing, was transferred into a preheated oven to facilitate further film growth. Removal of the Zn_2(ZnTCPP) film from the oven was followed by washing with fresh DMF and ethanol. The final step was to dry it under vacuum.

GIXRD patterns reveal that Zn_2(ZnTCPP) MOF films could be successfully grown on differently functionalised solid surfaces, *i.e.*, blank substrates, carboxyl-terminated and hydroxyl-terminated self-assembled monolayer (SAM) substrates by adopting the VAC method (Fig. S2†). The SAM functionalised substrates were obtained upon immersion of substrates in 1-mercaptoundecanol (MUD) and 16-mercaptohexadecanoic acid (MHDA) for at least 24 h at room temperature. According to the GIXRD patterns, the obtained Zn_2(ZnTCPP) films demonstrated bulk phase purity with high crystallinity for all substrates, after subjecting to a 3 h aging process under an 80 °C vapour exposed environment. Under identical conditions, the PP-MOF films deposited on solid substrates functionalised with –COOH and/or –OH groups exhibit a strong XRD peak intensity when compared with the PXRD pattern of a film cast on an analogous substrate with no functionalisation. The results suggest that PP-MOF films have better crystallinity on functionalised substrates than on the non-functionalised substrates. This can be attributed to the induction ability of functional groups during the nucleation step in PP-MOFs. Whilst nucleating, the functional groups facilitate Zn(II) ions to be anchored on the surface *via* coordination bonds.[3,31] Thereafter, these coordinated Zn(II) can serve as a metal source during the PP-MOF film growth. In contrast, in the non-functionalised surfaces, weak interactions like hydrogen bonding and van der Waals interactions between the surface and Zn(II) ions suffer from an equilibrium process during the nucleation step. This hinders the subsequent growth process, resulting in low crystallinity.[32] In the VAC-assisted growth process, the resulting PP-MOF films exhibit a preferred orientation [001] which is independent of surface anchored functional groups.

In the solvothermal method, the Zn_2(ZnTCPP) film was grown on a typical –COOH functionalised gold substrate in a reactant solution composed of $Zn(NO_3)_2 \cdot 6H_2O$, TCPP and modulator acetic acid, in a binary mixture of DMF and ethanol (v/v, 3/1) at 80 °C for one day. The GIXRD patterns in Fig. 1a suggest a random orientation of the surface-grown Zn_2(ZnTCPP) film. This is evidenced by a predominant reflection along [001] with several weak peaks appearing at (110), (200) and (400). This is indicative of the big challenges associated with the fabrication of a perfectly oriented 2D PP-MOF film, if solvothermal method is pursued.

Regarding the modular assembly method, Zn_2(ZnTCPP) nanosheets were synthesised first and ultrasonically dispersed in ethanol to get a PP-MOF ink; the ink carefully placed on water exhibited a spontaneous spread-out. This afforded a thin film on top of the water surface due to its hydrophobicity, following which it was transferred to the substrates yielding a thin film *via* a stamping process. The as-prepared Zn_2(ZnTCPP) film displays a preferably oriented [001] growth at 17.6° with a lattice spacing of 1.007 nm (calculated from the Bragg equation, $n\lambda = 2d \sin\theta$). Only a slight shift (0.2°) appeared, on comparing with the films prepared *via* VAC, solvothermal and LPE methods (17.8° with a lattice spacing of 0.996 nm). The peak shift and lattice

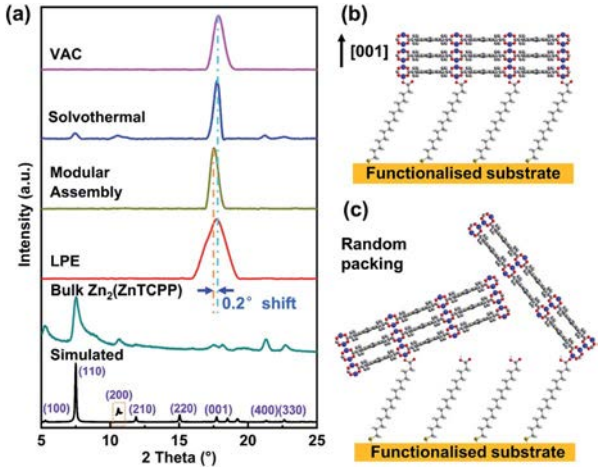

Fig. 1 (a) Simulated and experimental PXRD patterns of bulk Zn_2(ZnTCPP) and GIXRD patterns of the Zn_2(ZnTCPP) films fabricated by VAC, solvothermal, modular assembly and LPE methods (the inset is the magnified (200) peak); schematic illustration of the Zn_2(ZnTCPP) films grown along the [001] direction by (b) VAC, modular assembly, and LPE methods and (c) the solvothermal method leading to random packing. Relevant details: thin films were prepared on COOH functionalised gold substrates (1 cm × 1 cm) (VAC deposition was conducted using 30 μL of freshly prepared MOF precursor solution with acetic acid acting as the modulator at 80 °C for 3 h; modular assembly deposition was performed with five stamping cycles; LPE deposition was done over thirty consecutive cycles).

difference can be ascribed to the different film deposition strategies, each governed by distinct crystallisation equilibrium processes from the other. Modular assembly is a top-down deposition technique, in which the film composed of 2D Zn_2(-ZnTCPP) nanosheets is ultrasonically stripped from the bulk Zn_2(ZnTCPP).[19] Ultrasonication is likely to disintegrate the weak interlayer interactions, *vis-à-vis* to increase the interlayer space between the nanosheets.

For the Zn_2(ZnTCPP) film growth using LPE, the –COOH functionalised substrate was immersed in $Zn(OAC)_2 \cdot 2H_2O$ and TCPP solutions in an alternating manner, with an ethanol washing step performed in between two consecutive reaction steps. According to the GIXRD pattern in Fig. 1a, a crystalline Zn_2(ZnTCPP) film with the preferred orientation along the [001] direction was obtained. This disclosed the feasibility of LPE to grow 2D Zn_2(ZnTCPP) films on functionalised substrates. Our observation of several strong (*hk*0) peaks (*viz.*, (100), (110), (200), (400) and (330)) in the in-plane XRD patterns and (001) peaks in the GIXRD patterns confirmed the high crystallinity and perfect orientation of the Zn_2(ZnTCPP) films grown by VAC, modular assembly and LPE methods; however, the in-plane XRD and GIXRD patterns of the solvothermally prepared Zn_2(ZnTCPP) film included the characteristic (001) peak, suggestive of the random nature of film growth (Fig. 1 and S3†).[19]

Attenuated total reflection infrared spectroscopy (ATR-IR) spectra and ultraviolet-visible spectroscopy (UV-Vis) spectra were also recorded to confirm the compositions of the PP-MOF films, prepared by all four deposition techniques. The free H_2TCPP ligands were metalated during the growth of the Zn_2(ZnTCPP) film as evidenced by disappearance of the N–H stretching vibration at 960 cm^{-1} and appearance of a new peak at 996 cm^{-1}. This could be assigned to Zn–N bonds (Fig. S4†).[25,33] Moreover, compared to the spectrum of H_2TCPP, the spectrum of Zn_2(ZnTCPP) films indicated peaks disappearing around 1700 and 1270 cm^{-1} and two new strong peaks appearing around 1625 cm^{-1} and 1400 cm^{-1}. These synchronous disappearance and emergence of IR stretching signatures indicate coordination of the TCPP carboxylate groups to the Zn(II) atoms.[19,33]

The UV-Vis spectrum of the H_2TCPP ligand presents a strong Soret band at 411 nm together with four Q-bands at 525, 565, 590, and 652 nm (Fig. S5†). The Soret band of Zn_2(ZnTCPP) films was noticed to undergo a red shift to 428 nm, and two weak Q bands red-shifted to 567 and 603 nm, respectively. This confirmed the metalation of porphyrin rings by Zn(II) during the reaction process.[25]

SEM images identified differences in morphologies among the differently prepared PP-MOF films, suggesting variations that must have occurred during the nucleation and growth of the PP-MOF crystallites onto the –COOH terminated gold surface.[34] The Zn_2(ZnTCPP) film prepared by VAC shows a smooth, dense and homogeneous distribution with a grain size of ~200 nm (Fig. 2a and b). By controlling the stoichiometry of acetic acid serving as the reaction modulator, morphologies

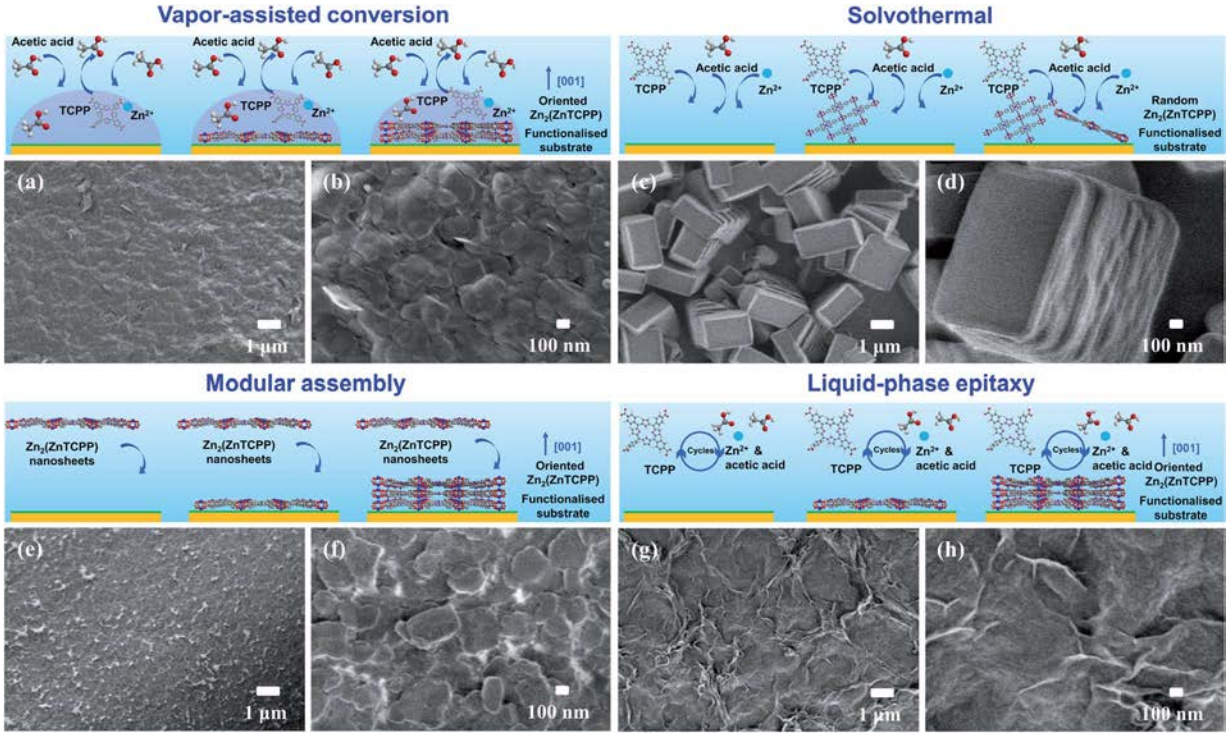

Fig. 2 SEM images of Zn_2(ZnTCPP) films fabricated by (a, b) VAC, (c, d) solvothermal, (e, f) modular assembly and (g, h) LPE methods; the proposed nucleation and growth processes involved in each method are schematically illustrated on top of these SEM images. All films were prepared on the COOH functionalised gold substrates (1 cm × 1 cm) (relevant details: VAC deposition was performed using 30 μL of freshly prepared MOF precursor solution with acetic acid as the modulator, at 80 °C for 3 h; modular assembly deposition was conducted with five consecutive stamping cycles; LPE deposition was done over thirty consecutive cycles).

of Zn_2(ZnTCPP) film could be fine-tuned. For example, a crystalline film with a flat and rough layer on the solid surface could be obtained by excluding the use of acetic acid, featuring a rectangular nanosheet morphology ~500 nm, each (Fig. S6 and S7†). A similar phenomenon was observed in the films prepared without acetic acid and DMF (Fig. S8 and S9†). The carboxylic acid groups in acetic acid are anticipated to selectively coordinate to Zn(II) ions, serving as the nucleation modulator during the growth of the 2D PP-MOF.[25,35] In the initial stage, such a modulator is known to compete with the TCPP ligand while coordinating to Zn(II) ions, leading to a 2D structure along the *ab* plane. This competition is supposed to slow down the nucleation of Zn_2(ZnTCPP) nanosheets. Meanwhile, acetic acid easily coordinated to Zn(II), to elicit steric hindrance impeding the isotropic growth of Zn_2(ZnTCPP) along the *c* axis.[25,36] Thus, the Zn_2(ZnTCPP) film with small nanosheets could be obtained. Besides, the thickness of films grown *via* VAC could be controlled facilely by using different amounts of the precursor solution for VAC growth (Fig. S10†).

In contrast, the films solvothermally grown exhibit random packing behaviour as opposed to being chemically anchored onto the surface (Fig. 2c and d). This is because Zn_2(ZnTCPP) with a simple 2D "checkerboard" structure can be formed rapidly and the abundant 2D layers in proximity could interact to get aligned. Such an alignment could facilitate growth and self-packing along the *c*-axis rather than precise nucleation on the substrate surface. Most of the PP-MOF crystallites could be observed along the *ab* plane ([001] oriented growth) accompanied by a small amount of other faces. This indicates a lack of preference in the orientation of film growth. These results are in agreement with the GIXRD profiles. Thanks to modular assembly, a smooth and homogeneous surface of the Zn_2(ZnTCPP) film could be obtained (Fig. 2e and f). Because of the ultrasonic stripping of the Zn_2(ZnTCPP) nanosheets from the bulk form, a small size (~300 nm), high-aspect-ratio flaky morphology could be accessed. Such a controlled assembly process enables us to prepare dense and packed nanofilms (Fig. 2e and f). The film thickness can be manipulated by adjusting the number of deposition cycles.[19] Meanwhile, powered by our command on the concentrations of precursor solutions and on the number of deposition cycles, LPE offers the advancement to nucleate small sites and grow a uniform film of high topical interest (Fig. 2g and h). The beauty of the LPE method lies in the fact that it allows the MOF films to grow with a precisely controlled nanoscale thickness, guided by a regulated number of deposition cycles.[26] In simple terms, VAC, modular assembly and LPE methods feature advantages such as precise engineering of the nucleation and growth processes for fabricating uniform 2D PP-MOF films with fine-tuned thickness, whereas the solvothermal approach works well for nucleation with difficulties to control their morphology and thickness.

Evaluation of surface roughness by determining the arithmetic average roughness (R_a) and the root mean squared roughness (R_q) (Table S3†) confirmed flatness of the differently prepared films (Fig. S11†).[37–39] The Zn_2(ZnTCPP) films prepared by VAC and LPE exhibit surface roughness profiles (Fig. S11a and d†) with R_a values of 4.5 nm and 2.9 nm, respectively. In modular assembly, the film is characterised with an acceptable roughness profile, $R_a = 8.1$ nm (Fig. S11c†). Consistent with the SEM image, the film grown *via* the solvothermal method exhibits roughness (Fig. S11b†) with a much higher R_a, ~54.1 nm; a plausible outcome of the random packing of bulk Zn_2(ZnTCPP) crystallites.

2.2. Preparation and characterisation of 3D PP-MOF films

Zirconium-based porphyrinic MOFs (Zr-MOFs) are typical representatives of 3D PP-MOFs.[40–42] They feature extraordinary chemical stability, a wide range of pore sizes, and excellent (photo)electrocatalytic properties, ideally suited for a wide range of applications, such as solar cells, chemical sensors and photo/electrocatalysis.[7,8,43,44] Similar to the studies on 2D PP-MOF films, VAC, solvothermal, modular assembly and LPE methods were implemented to prepare 3D PP-MOF films. PCN-222, PCN-224 and MOF-525 can result from the coordination of the TCPP ligand with the Zr_6 cluster but they exhibit different network topologies and pore architectures, an artefact of the intrinsic differences in the metal–organic coordination numbers and symmetries of the Zr_6 clusters composing the frameworks (Fig. S12†).[40–42] A set of identical structural connectors *i.e.* links and different framework topologies could afford the distinct 3D structures of PCN-222, PCN-224 and MOF-525, making them comparable examples. A coherent study of such analogues helps us to understand the nucleation and growth processes in prototypal 3D PP-MOF films cast on different solid surfaces, and the outcomes of different deposition routes associated therein.

We began to study the VAC assisted growth of PCN-222 films on –COOH functionalised substrates. GIXRD patterns of PCN-222 films confirmed their phase purity and high crystallinity (Fig. S13†). Unlike the 2D Zn_2(ZnTCPP) nanosheets, the oriented growth of 3D PCN-222 crystallites favours their formation on the functional group modified substrates. A highly oriented film along the [100] direction was obtained on the –COOH functionalised gold surface. However, the PCN-222 films that grew upon silicon wafer and ITO glass showed two weak peaks at ~6.6° and 8.3°, corresponding to the [211] and [420] orientations, respectively. These results suggest randomly oriented growth of these films. The growth mechanism of the oriented PCN-222 on the –COOH functionalised gold surface is illustrated in Fig. 3b. During the reaction, Zr(IV) metal ions nucleate to form the Zr_6 clusters. The carboxylic groups of the SAM functionality selectively coordinate to these Zr_6 clusters subsequently, anchoring the metal clusters on the surface. Following this, TCPP linkers coordinate to the Zr_6 clusters inducing the "oriented/layered" growth of PCN-222 along the *bc* plane, parallel to the substrate. This in turn contributes to the further nucleation and growth along the *a* axis (Fig. S14†).[14] The functional organic groups of the SAM on the substrate surface offer a few advantages to facilitate selective nucleation and oriented growth of PP-MOF films, whereas favourable reaction conditions are also deemed crucial for film fabrication purposes.

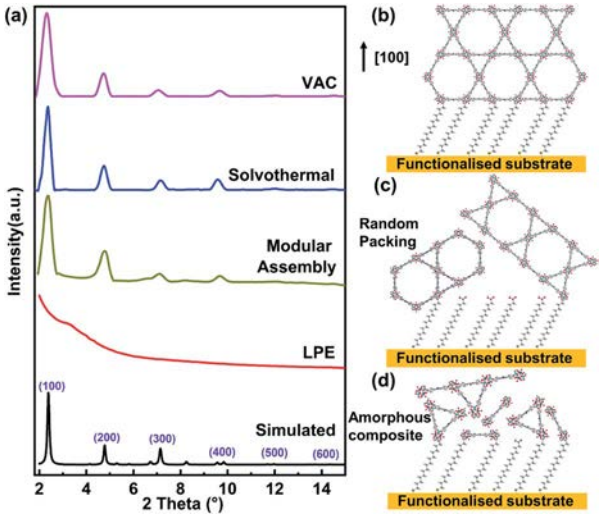

Fig. 3 (a) Simulated PXRD pattern of bulk PCN-222 and GIXRD patterns of PCN-222 films fabricated by VAC, solvothermal, modular assembly and LPE methods; schematic illustration of the PCN-222 films grown along the [100] direction by (b) VAC and solvothermal methods, and (c) the modular assembly method leading to random packing, and (d) growth of amorphous composites *via* LPE. Relevant details: thin films were prepared on COOH functionalised gold substrates (1 cm × 1 cm) (VAC deposition was conducted using 30 μL of freshly prepared MOF precursor solution with acetic acid as the modulator (r_M 219) at 100 °C for 3 h; modular assembly deposition was performed with five stamping cycles; LPE deposition was done over thirty consecutive cycles).

To obtain further insights into the VAC assisted growth of PCN-222 films, we separately investigated the impacts of modulator concentration, precursor concentration, reaction time, reaction temperature, and droplet volume on the crystallinity, morphology and thickness. This was done by altering the synthesis conditions (Table S4†). Even a slight change to the amount of modulator in the form of acetic acid can result in differences in crystallinity, morphology, and orientation of the PP-MOF films, reiterating the vital role played by a modulator during the fabrication of a PP-MOF film. As shown in Fig. S15,† the obtained PCN-222 films display relatively poor crystallinity in the form of weak GIXRD peaks when the modulator/metal salt ($ZrOCl_2 \cdot 8H_2O$) concentration ratio (r_M) was below 219. PCN-222 films with a good orientation and crystallinity were formed with an r_M of 219 to 437. By adjusting the modulator and upon further controlling the r_M from 437 to 874, phase transition from PCN-222 to PCN-224 could be noted in the PP-MOF. Mediated by the modulator adjustment, grain size in PCN-222 increased from an r_M of 219 to 437 (Fig. S16†). This is because low concentration of modulator results in a fast nucleation and crystallisation process, which is in agreement with the literature reports.[7,45] High precursor concentration resulted in the randomly oriented growth of the PCN-222 film, accessed *via* VAC (Fig. S17†). The plausible reason is the abundance of reactants which induces fast nucleation in the precursor solution and exacerbates the difficulty in controlling the oriented growth followed by nucleation on functionalised substrate surfaces. An adequate reaction time is important to efficiently sustain nucleation and crystalline growth. Herein, we find that a reaction time of only 3 h was sufficient to afford the PCN-222 films and a prolonged reaction time of 12 h did not bring any change: a pure and crystalline phase was retained (Fig. S18†). Reaction temperature is also vital for the nucleation and crystallisation of PP-MOF films. For PCN-222, a highly crystalline and oriented film was obtained at 100 °C, whereas a low temperature of 80 °C resulted in a considerable loss of crystallinity in the PCN-222 film (Fig. S19†).

To better understand the nucleation and growth processes of the 3D PP-MOF film, similar to our foregoing studies on the 2D analogues, modular assembly, LPE and solvothermal methods were used to fabricate the PCN-222 films to comparatively analyse their crystallinity, morphology and thickness. As shown in Fig. 3, GIXRD patterns confirmed that a crystalline PCN-222 film with an oriented growth could be solvothermally prepared. Upon comparing this result to 2D Zn_2(ZnTCPP), it appears that the more complex 3D MOF architecture of PCN-222 and a higher amount of modulator used in its synthesis process could slow down the reaction rate, leveraging opportunities for selective and precise nucleation on the surface-localised functional groups.[35] When deposited by modular assembly, the PCN-222 film displays good crystallinity compared to those prepared solvothermally. In fact, modular assembly could not achieve an oriented growth of the PCN-222 film, evident from the weak nature of the two GIXRD peaks at 6.6° and 8.3°. The random orientation of the 3D PP-MOF film is attributed to the rod-like PCN-222 crystallites (Fig. 4e and f). Compared to the modularity and high-aspect-ratio flaky structure of the 2D PP-MOF congener, in its 3D form, forming an oriented film by controlling the crystallite orientation becomes increasingly difficult.[19,46] The GIXRD pattern of the PCN-222 film fabricated by LPE did not reveal any characteristic peak, thus suggesting the formation of amorphous PCN-222. The plausible explanation might be the high energy barrier of formation in cases of such complicated and symmetric 3D topology structures (**csq** for PCN-222), which lie beyond the reach of LPE operating under relatively mild conditions.[40,46,47] To be specific, during the MOF crystallisation process, secondary building units (SBUs) are formed initially. Credited to this direct supply of pre-synthetic SBUs, the nucleation kinetics gets accelerated in order to reduce the energy barrier of MOF crystallisation.[48,49] However, for 3D PP-MOFs like PCN-222, growth of a crystalline film evidently fails with the introduction of Zr_6 cluster-based SBUs as the metal resource, under the mild conditions of LPE. This seems a shortcoming of LPE, considering the scope of growing the 3D films of PCN-222.

Thin films grown by all the aforementioned methods present similar ATR-IR spectra (Fig. S20†). Compared to the spectrum of the CuTCPP ligand, PCN-222 films exhibit the absence of peaks around 1700 cm^{-1} and 1270 cm^{-1} whereas the peak enhanced at 1400 cm^{-1} is reflective of the carboxyl coordination in CuTCPP to the Zr(IV) centres. This also suggests that the TCPP ligands despite coordinating to Zr_6 SBUs failed to form a crystalline PP-MOF during the LPE film growth process.

As shown in Fig. 4, SEM images of PCN-222 films fabricated by different methods were studied. Top-view SEM images reveal

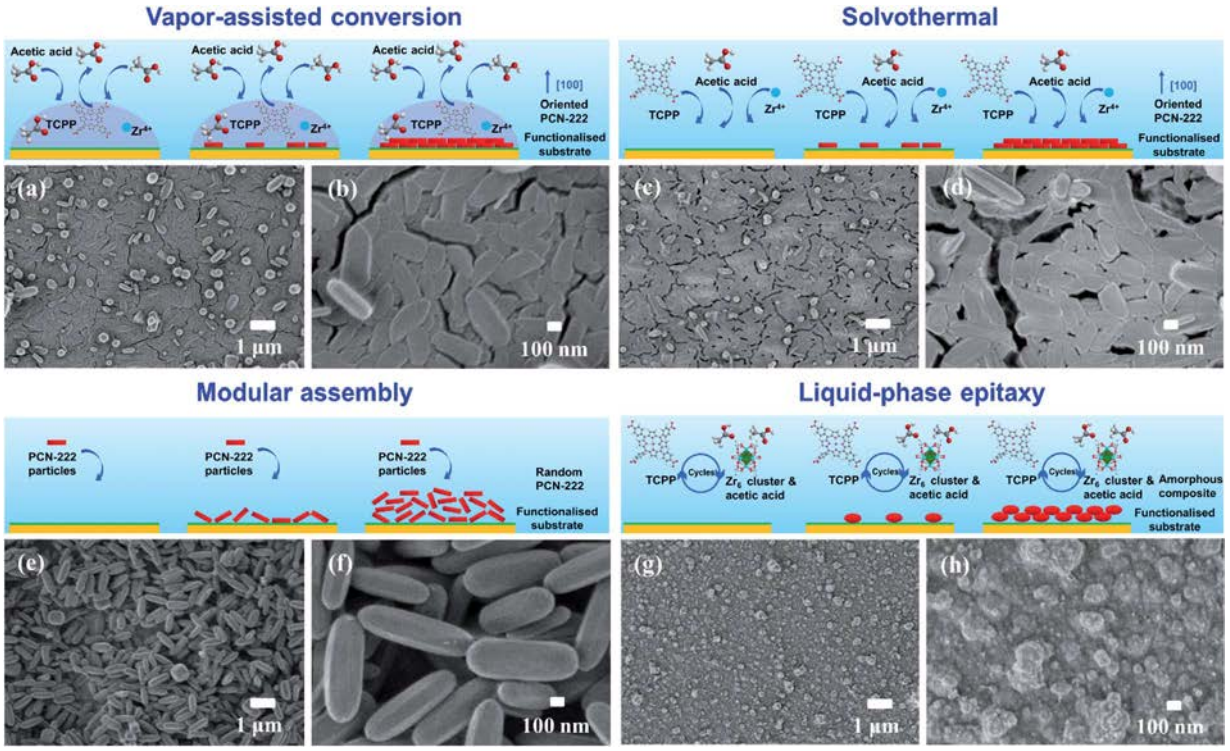

Fig. 4 SEM images of PCN-222 films fabricated by (a, b) VAC, (c, d) solvothermal, (e, f) modular assembly and (g, h) LPE methods; the proposed nucleation and growth processes involved in each method are schematically illustrated on top of these SEM images. All films were prepared on the COOH functionalised gold substrates (1 cm × 1 cm) (relevant details: VAC deposition was performed using 30 μL of freshly prepared MOF precursor solution with acetic acid as the modulator (r_M 219 eq.), at 100 °C for 3 h; modular assembly deposition was conducted with five consecutive stamping cycles; LPE deposition was done over thirty consecutive cycles).

that VAC could assemble a highly smooth, dense and homogeneous PCN-222 film on the solid surface (Fig. 4a and b) with a controlled thickness (Fig. S21†). High surface coverage of this film indicates its tendency towards anchoring with the –COOH functionalised substrates. Identification of PCN-222 crystallites with two different grain sizes on top of the film confirmed the coexistence of two individual nucleation processes accompanying the film growth. First, a heterogeneous nucleation was initiated on the solid surface and then a homogeneous nucleation occurred in the liquid volume left on the film surface.[23] The homogeneous nucleation could be plausibly attributed to a change in the ratio of reactants that occupied the remaining liquid volume. Similarly, the solvothermally grown PCN-222 film exhibits a smooth, dense and homogeneous morphology with intergrown rod-shaped crystallites. All these rod-shaped crystallites aligned in parallel to the substrate plane *i.e.* along the *a* axis. This matches well with the GIXRD pattern, providing evidence of the [100] reflection. The 3D PCN-222 film prepared by modular assembly exhibited a rough surface with random rod crystallites densely packed on the substrate. This is much different from the smooth and flat surface of 2D PP-MOF films obtained with high-aspect-ratio flaky nanosheets. Consistent with the XRD pattern (Fig. 3), the film grown *via* LPE was amorphous on the substrate surface. This is due to a high energy barrier of crystallisation for PCN-222, under the mild LPE immersion conditions. SEM images of the PCN-222 films prepared by VAC on silicon and ITO substrates exhibited a similar morphology: a smooth, dense, and homogeneous surface (Fig. S22†), more specifically.

Surface roughness of the differently prepared PCN-222 films was also investigated (Fig. S23†). In agreement with the SEM images, each of the films grown *via* VAC and solvothermal methods presents a smooth surface with low roughness ($R_a \sim$ 2.2 nm and 3.6 nm, respectively, Table S5†). In contrast, the film prepared by modular assembly presents a higher but acceptable surface roughness. Despite our failure to obtain a crystalline PCN-222 film, this amorphous film obtained *via* LPE reveals a smooth surface, characterised by a low $R_a \sim 4.0$ nm.

To obtain further insights into the feasibility of utilising VAC in the fabrication of 3D PP-MOF films, *viz.* PCN-224 and MOF-525 with distinct framework topologies and structures, they were also grown on the –COOH functionalised gold substrates with the help of VAC (see Tables S6 and S7† for details).

For the PCN-224 film on functionalised surfaces, a preferred crystallite orientation along the [200] direction could be found (Fig. S24 and S25†). The influence of varying modulator concentrations on the formation of PCN-224 films could also be examined. According to the GIXRD pattern, when the r_M is 437, the reaction system yielded a randomly oriented PCN-224 phase (with little PCN-222 phase). In contrast, an oriented and crystalline PCN-224 film was obtained with a ratio of 874 (Fig. S26†). This observed random orientation in PCN-224 at 437 eq. of modulator concentration could be attributed to the fast nucleation process occurring at low modulator levels, followed by an

imprecise control over the growth orientation. Moreover, similar to the PCN-222 film formation, a mere 3 h reaction time was found enough for the nucleation and growth of a crystalline and oriented PCN-224 film. When the duration was prolonged to 12 h, the film obtained failed to strike any difference from the one obtained after 3 h (Fig. S27†). The impact of reaction temperature was studied as well; the GIXRD patterns suggested that high temperature could induce a randomly oriented growth in the film (Fig. S28†). This might be attributed to the faster nucleation process and a concomitant loss of precise control over the oriented film growth processes at high temperatures, prompted by selective nucleation.

The SEM images and roughness profile indicate a smooth, dense, homogeneous and crystalline PCN-224 film fabricated *via* VAC on a solid surface (Fig. S29, S30 and Table S8†). The magnified version of SEM reveals the dense growth of cubic crystallites, all of uniform size. The sporadic MOF crystallites on top of the film are due to a secondary nucleation process.

Regarding the VAC assisted fabrication of MOF-525 films on a functionalised gold substrate, unlike PCN-222 and PCN-224, no preferred crystallite orientation was noted in the MOF-525 films (Fig. S31 and S32†). This is plausibly ascribed to the fully bridged 12-connecting Zr_6 clusters which results in a myriad of choices while nucleating and while getting aligned as part of the film growth *i.e.* when the clusters get anchored on the terminal organic groups of the SAM on solid surfaces.

As shown in Fig. S33,† GIXRD patterns indicate that the MOF phase changes slightly from PCN-222 to MOF-525 with an increase in the modulator concentration. When the r_M is at or below 219, crystalline PCN-222 phase films were obtained even at a low Zr/TCPP reactant ratio (Zr/TCPP was 2/1 for MOF-525, and Zr/TCPP was 3/1 for PCN-222, corresponding to their compositional ratios in the respective MOF structures). When the modulator concentration was in between 365 eq. and 584 eq. of $ZrOCl_2 \cdot 8H_2O$, the film appeared to be a mixed MOF phase of PCN-222 and MOF-525. A crystalline MOF-525 film could be obtained with $r_M \sim 730$, but with random orientation. Despite the high symmetry of MOF-525, crystalline films resulted within 3 hours. The morphology and nature of this film remained unchanged even after subjecting to a prolonged reaction time of 12 h (Fig. S34†). These SEM results are indicative of the propensity of our pursued VAC method to afford dense, homogeneous and crystalline MOF-525 films. The MOF-525 crystallites were found packed on the –COOH functionalised gold substrate with a random orientation, consistent with the GIXRD pattern (Fig. S35†).

That a prototypal class of 3D PP-MOF films, comprising similar porphyrin linkers and metal ion based clusters, are amenable to solid surface fabrication by fine-tuning the modulator content becomes evident from our foregoing experimental results.

2.3. Adsorption properties of differently fabricated PP-MOF films

As discussed above, the crystallinity, morphology and thickness of the PP-MOF films are controlled to a large extent by the preparation method(s) involved. Meanwhile, the preparation conditions affording the PP-MOF films play a key role in controlling their properties. Treating vapour adsorption properties as our studied properties amenable to film growth based fine-tuning, ample scope to examine the distinctly prepared thin films' sorption features remains. Upon recording vapour sorption isotherms using an environmentally controlled QCM detector, the prepared series of 2D and 3D PP-MOF films revealed interesting trends as discussed in the following.

For the 2D PP-MOFs, each of the four distinctly prepared Zn_2(ZnTCPP) films were marked with a typical type I Langmuir isotherm for methanol vapour at 25 °C (Fig. 5a). These isotherms are signatures of their microporosity and suggest that facile diffusion of methanol occurs into each of their polar pores replete with carboxyl groups. The four films exhibit different methanol adsorption capacities at P/P_0 of 0.95, suggestive of their differing polar nature.[50] Compared to the solvothermally fabricated film showing an uptake of 3.5 mmol g^{-1} methanol vapour, the films obtained using modular assembly, LPE and VAC exhibited higher uptakes: 5.6 mmol g^{-1}, 6.3 mmol g^{-1} and 5.8 mmol g^{-1}, respectively. Apart from offering insights into their relative polar characteristics, this trend is in good agreement with the excellent crystallinity of the films. The lower methanol adsorption amount (3.5 mmol g^{-1}) of the solvothermally grown film can be ascribed well to the disparate growth of a randomly oriented bulk Zn_2(ZnTCPP) MOF on the substrate surface during the solvothermal process.[6]

In contrast to these similarly behaving 2D PP-MOFs, among the four distinctly prepared 3D PP-MOFs, two Zn_2(ZnTCPP) films *i.e.* the ones derived from LPE and modular assembly were noted to exhibit typical type I Langmuir isotherms for methanol vapour at 25 °C (Fig. 5b). Typical type IV isotherms were observed for the other two films fabricated *via* VAC and solvothermal techniques, marked with a steep increase at $P/P_0 \sim 0.3$, indicating their mesoporosity.[40] Compared to the films fabricated *via* LPE and modular assembly, the oriented PCN-222 films obtained *via* VAC and solvothermal methods demonstrated much higher amounts of adsorbed methanol, 19.8 mmol g^{-1} and 15.6 mmol g^{-1},

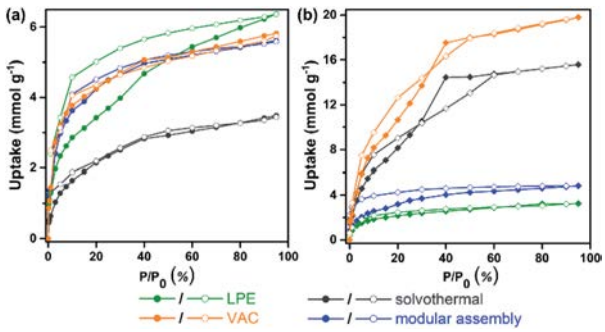

Fig. 5 Methanol vapour sorption isotherms at ambient temperature (25 °C) obtained using an environmentally controlled quartz crystal microbalance (BELQCM-4 equipment) of (a) Zn_2(ZnTCPP) and (b) PCN-222 films fabricated by VAC, solvothermal, modular assembly and LPE methods on the COOH functionalised Au-coated QCM substrates. Filled and open symbols denote adsorption and desorption, respectively.

respectively, at $P/P_0 \sim 0.95$. This is attributed to the oriented, smooth and dense morphology of the PCN-222 films grown by VAC and solvothermal methods, which offer more periodic, uniform and compact pores, thus leading to an enhanced adsorption property.[14,28,35] The lower methanol affinity (4.9 mmol g^{-1}) in the film fabricated *via* modular assembly is ascribed to the stacks of randomly oriented PCN-222 rod crystallites on the substrate surface.[14] Despite the absence of crystallinity, the LPE grown film exhibits a micropore filling of 3.2 mmol g^{-1} methanol uptake, an indication of its guest-accessibility. The PCN-224 film prepared *via* VAC shows a considerable methanol adsorption uptake (16.5 mmol g^{-1}) at 25 °C, proving the high porosity of the oriented PCN-224 film (Fig. S36†). The randomly oriented MOF-525 film exhibits 10.2 mmol g^{-1} methanol uptake (Fig. S37†).

3. Conclusions

In summary, we first developed VAC as a facile and versatile route to grow highly crystalline, smooth, dense, homogeneous and oriented films of both 2D and 3D PP-MOFs on various solid surfaces. Key details regarding the parameters associated with controlling the nucleation and growth of PP-MOF films, including the reactant and modulator concentration, droplet volume, reaction temperature and reaction time, have been investigated. Our study identifies the important role played by the modulator in prompting nucleation and facilitating oriented film growth. The obtained PP-MOF films reveal a considerable saturation uptake of methanol at room temperature, suggesting their high guest-accessible volumes and polar Connolly surfaces. Moreover, different methods (*viz.*, VAC, solvothermal, modular assembly and LPE) could be critically compared for easy understanding of the mechanism(s) behind PP-MOF film nucleation and growth. This study proposes to provide a point of reference for all future research studies revolving around the preparation of PP-MOF thin films.

Acknowledgements

Z. Y. Zhou and S. J. Hou are grateful for the PhD fellowship donated by the China Scholarship Council (CSC). W. J. Li and S. Mukherjee gratefully acknowledge the Alexander von Humboldt Foundation for each of their postdoctoral research fellowships. Z. Y. Zhou is grateful to Shanshan Yin and Prof. Peter Müller Buschbaum for providing the surface profile analysis data. This work was supported by the German Research Foundation (DFG) Priority Program 1928 "Coordination Networks: Building Blocks for Functional Systems".

Notes and references

1 S. Batten, N. Champness, X. Chen, J. Garcia-Martinez, S. Kitagawa, L. Öhrström, M. O'Keeffe, M. Suh and J. Reedijk, *Pure Appl. Chem.*, 2013, **85**, 1715.
2 P. Falcaro, R. Ricco, C. M. Doherty, K. Liang, A. J. Hill and M. J. Styles, *Chem. Soc. Rev.*, 2014, **43**, 5513.
3 J. Liu, W. Zhou, J. Liu, I. Howard, G. Kilibarda, S. Schlabach, D. Coupry, M. Addicoat, S. Yoneda, Y. Tsutsui, T. Sakurai, S. Seki, Z. Wang, P. Lindemann, E. Redel, T. Heine and C. Wöll, *Angew. Chem., Int. Ed.*, 2015, **54**, 7441.
4 D. Micheroni, G. Lan and W. Lin, *J. Am. Chem. Soc.*, 2018, **140**, 15591.
5 G. Xu, K. Otsubo, T. Yamada, S. Sakaida and H. Kitagawa, *J. Am. Chem. Soc.*, 2013, **135**, 7438.
6 M. Zhao, Y. Wang, Q. Ma, Y. Huang, X. Zhang, J. Ping, Z. Zhang, Q. Lu, Y. Yu, H. Xu, Y. Zhao and H. Zhang, *Adv. Mater.*, 2015, **27**, 7372.
7 C. Su, C. Kung, T. Chang, H. Lu, K. Ho and Y. Liao, *J. Mater. Chem. A*, 2016, **4**, 11094.
8 P. M. Usov, B. Huffman, C. C. Epley, M. C. Kessinger, J. Zhu, W. A. Maza and A. J. Morris, *ACS Appl. Mater. Interfaces*, 2017, **9**, 33539.
9 L. Dumée, L. He, M. Hill, B. Zhu, M. Duke, J. Schütz, F. She, H. Wang, S. Gray, P. Hodgson and L. Kong, *J. Mater. Chem. A*, 2013, **1**, 9208.
10 D. Jiang, A. D. Burrows, Y. Xiong and K. J. Edler, *J. Mater. Chem. A*, 2013, **1**, 5497.
11 W. Li, M. Tu, R. Cao and R. A. Fischer, *J. Mater. Chem. A*, 2016, **4**, 12356.
12 W. Li, S. Xue, S. Watzele, S. Hou, J. Fichtner, A. L. Semrau, L. Zhou, A. Welle, A. S. Bandarenka and R. A. Fischer, *Angew. Chem., Int. Ed.*, 2020, **59**, 5837.
13 S. Wannapaiboon, M. Tu and R. A. Fischer, *Adv. Funct. Mater.*, 2014, **24**, 2696.
14 S. M. Yoon, J. H. Park and B. A. Grzybowski, *Angew. Chem., Int. Ed.*, 2017, **56**, 127.
15 C. W. Kung, T. H. Chang, L. Y. Chou, J. T. Hupp, O. K. Farha and K. C. Ho, *Chem. Commun.*, 2015, **51**, 2414.
16 P. M. Usov, S. R. Ahrenholtz, W. A. Maza, B. Stratakes, C. C. Epley, M. C. Kessinger, J. Zhu and A. J. Morris, *J. Mater. Chem. A*, 2016, **4**, 16818.
17 R. Makiura, S. Motoyama, Y. Umemura, H. Yamanaka, O. Sakata and H. Kitagawa, *Nat. Mater.*, 2010, **9**, 565.
18 S. Motoyama, R. Makiura, O. Sakata and H. Kitagawa, *J. Am. Chem. Soc.*, 2011, **133**, 5640.
19 G. Xu, T. Yamada, K. Otsubo, S. Sakaida and H. Kitagawa, *J. Am. Chem. Soc.*, 2012, **134**, 16524.
20 J. Liu, W. Zhou, J. Liu, Y. Fujimori, T. Higashino, H. Imahori, X. Jiang, J. Zhao, T. Sakurai, Y. Hattori, W. Matsuda, S. Seki, S. K. Garlapati, S. Dasgupta, E. Redel, L. Sun and C. Wöll, *J. Mater. Chem. A*, 2016, **4**, 12739.
21 D. J. Li, Z. G. Gu, I. Vohra, Y. Kang, Y. S. Zhu and J. Zhang, *Small*, 2017, **13**, 1604035.
22 M. C. So, S. Jin, H.-J. Son, G. P. Wiederrecht, O. K. Farha and J. T. Hupp, *J. Am. Chem. Soc.*, 2013, **135**, 15698.
23 E. Virmani, J. M. Rotter, A. Mähringer, T. von Zons, A. Godt, T. Bein, S. Wuttke and D. D. Medina, *J. Am. Chem. Soc.*, 2018, **140**, 4812.
24 Y. Wang, M. Zhao, J. Ping, B. Chen, X. Cao, Y. Huang, C. Tan, Q. Ma, S. Wu, Y. Yu, Q. Lu, J. Chen, W. Zhao, Y. Ying and H. Zhang, *Adv. Mater.*, 2016, **28**, 4149.

25 Y. Zhao, L. Jiang, L. Shangguan, L. Mi, A. Liu and S. Liu, *J. Mater. Chem. A*, 2018, **6**, 2828.
26 Y. Wang, S. Chen, R. Haldar, C. Wöll, Z. Gu and J. Zhang, *Adv. Mater. Interfaces*, 2018, **5**, 1800985.
27 E. Y. Choi, C. A. Wray, C. Hu and W. Choe, *CrystEngComm*, 2009, **11**, 553.
28 Z. Wang, K. Rodewald, R. Medishetty, B. Rieger and R. A. Fischer, *Cryst. Growth Des.*, 2018, **18**, 7451.
29 D. Zacher, A. Baunemann, S. Hermes and R. A. Fischer, *J. Mater. Chem.*, 2007, **17**, 2785.
30 K. M. Ishihara and F. Tian, *Langmuir*, 2018, **34**, 15689.
31 B. Liu, O. Shekhah, H. K. Arslan, J. Liu, C. Wöll and R. A. Fischer, *Angew. Chem., Int. Ed.*, 2012, **51**, 807.
32 S. Hermes, D. Zacher, A. Baunemann, C. Wöll and R. A. Fischer, *Chem. Mater.*, 2007, **19**, 2168.
33 M. Tian, F. Pei, M. Yao, Z. Fu, L. Lin, G. Wu, G. Xu, H. Kitagawa and X. Fang, *Energy Storage Materials*, 2019, **21**, 14.
34 J. Liu and C. Wöll, *Chem. Soc. Rev.*, 2017, **46**, 5730.
35 S. Wannapaiboon, K. Sumida, K. Dilchert, M. Tu, S. Kitagawa, S. Furukawa and R. A. Fischer, *J. Mater. Chem. A*, 2017, **5**, 13665.
36 T. Tsuruoka, S. Furukawa, Y. Takashima, K. Yoshida, S. Isoda and S. Kitagawa, *Angew. Chem., Int. Ed.*, 2009, **48**, 4739.
37 Y. Huang, C. A. Tao, R. Chen, L. Sheng and J. Wang, *Nanomaterials*, 2018, **8**, 676.
38 W. Yin, C. A. Tao, F. Wang, J. Huang, T. Qu and J. Wang, *Sci. China Mater.*, 2018, **61**, 391.
39 W. Yin, C. A. Tao, X. Zou, F. Wang, T. Qu and J. Wang, *Nanomaterials*, 2017, **7**, 242.
40 D. Feng, Z. Y. Gu, J. R. Li, H. L. Jiang, Z. Wei and H. C. Zhou, *Angew. Chem., Int. Ed.*, 2012, **51**, 10307.
41 D. Feng, W. C. Chung, Z. Wei, Z. Y. Gu, H. L. Jiang, Y. P. Chen, D. J. Darensbourg and H. C. Zhou, *J. Am. Chem. Soc.*, 2013, **135**, 17105.
42 W. Morris, B. Volosskiy, S. Demir, F. Gandara, P. L. McGrier, H. Furukawa, D. Cascio, J. F. Stoddart and O. M. Yaghi, *Inorg. Chem.*, 2012, **51**, 6443.
43 M. Oldenburg, A. Turshatov, D. Busko, S. Wollgarten, M. Adams, N. Baroni, A. Welle, E. Redel, C. Woll, B. S. Richards and I. A. Howard, *Adv. Mater.*, 2016, **28**, 8477.
44 H. Q. Xu, J. Hu, D. Wang, Z. Li, Q. Zhang, Y. Luo, S. H. Yu and H. L. Jiang, *J. Am. Chem. Soc.*, 2015, **137**, 13440.
45 G. Zahn, H. A. Schulze, J. Lippke, S. König, U. Sazama, M. Fröba and P. Behrens, *Microporous Mesoporous Mater.*, 2015, **203**, 186.
46 Z. Fu and G. Xu, *Chem. Rec.*, 2017, **17**, 518.
47 D. Feng, Z. Y. Gu, Y. P. Chen, J. Park, Z. Wei, Y. Sun, M. Bosch, S. Yuan and H. C. Zhou, *J. Am. Chem. Soc.*, 2014, **136**, 17714.
48 D. Zacher, R. Schmid, C. Wöll and R. A. Fischer, *Angew. Chem., Int. Ed.*, 2011, **50**, 176.
49 O. Shekhah, H. Wang, D. Zacher, R. A. Fischer and C. Wöll, *Angew. Chem., Int. Ed.*, 2009, **48**, 5038.
50 S. Mukherjee, A. V. Desai and S. K. Ghosh, *Coord. Chem. Rev.*, 2018, **367**, 82.